

Universal Quantum Control through Deep Reinforcement Learning

Murphy Yuezhen Niu,^{1,2,*} Sergio Boixo,^{3,†} Vadim Smelyanskiy,^{3,‡} and Hartmut Neven^{3,§}

¹*Research Laboratory of Electronics, Massachusetts Institute of Technology, Cambridge, Massachusetts 02139, USA*

²*Department of Physics, Massachusetts Institute of Technology, Cambridge, Massachusetts 02139, USA*

³*Google, 340 Main Street, Venice Beach, California 90291, USA*

(Dated: April 17, 2018)

Emerging reinforcement learning techniques using deep neural networks have shown great promise in control optimization. They harness non-local regularities of noisy control trajectories and facilitate transfer learning between tasks. To leverage these powerful capabilities for quantum control optimization, we propose a new control framework to simultaneously optimize the speed and fidelity of quantum computation against both leakage and stochastic control errors. For a broad family of two-qubit unitary gates that are important for quantum simulation of many-electron systems, we improve the control robustness by adding control noise into training environments for reinforcement learning agents trained with trusted-region-policy-optimization. The agent control solutions demonstrate a two-order-of-magnitude reduction in average-gate-error over baseline stochastic-gradient-descent solutions and up to a one-order-of-magnitude reduction in gate time from optimal gate synthesis counterparts.

INTRODUCTION

Designed to exert the full computational force of Nature, quantum computers utilize the laws of quantum mechanics to explore the exponential computational space in superposition. A critical step that connects theory to experiment is the careful design of quantum controls to translate each quantum algorithm into a set of analog control signals that accurately steer the quantum computer around the Hilbert space. The precise choice of these controls ultimately governs the fidelity and speed of each quantum operation.

The fidelity and runtime of quantum gates are crucial measures of quantum control that determines the computational capacity of both near- and long-term quantum devices. Higher gate fidelities lower the resource overhead for fault-tolerant error correction, while shorter runtimes directly extend quantum circuit depth by racing to avoid the onset of uncorrectable errors caused by noise and dissipation [1].

Another key component that determines the practical applications of near-term quantum devices is the universality of the quantum gates realizable through analog controls. For pre-fault-tolerant quantum computers, quantum operations are not limited to a finite gate set otherwise necessary for achieving fault-tolerance. Consequently, implementing high-fidelity and fast quantum gate with one control pulse sequence

instead of a long depth circuit through optimal gate synthesis approach can greatly reduce the resource overhead and expand the feasible computational tasks. As recently demonstrated in Refs. [2, 3], replacing the standard universal gate set with unrestricted unitary gates reduces the required circuit depth for the near-term demonstration of quantum supremacy in experiment by one order of magnitude.

However, a universal control framework that facilitates optimization over major experimental non-idealities under systematic constraints has been lacking, which prevents us from fully leveraging the flexibility of quantum control schemes. On the one hand, quantum computing systems with an ever-growing number of qubits are facing aggravating amounts of stochastic control errors and information leakage outside the computational subspace. On the other hand, the specific form of system Hamiltonians is limited by the underlying physics of the computing platform and thus unable to directly induce any desired quantum dynamical evolution on demand. Overcoming these challenges is key to reaping various computational speedups promised by quantum computers [2, 4, 5].

Stochastic control errors can severely perturb the actual control outcomes if not well accounted for during control optimizations. But in most cases, the exact model of experimental control errors is unavailable. Efforts towards improving control robustness against control errors have been centered around closed-loop feedback optimizations [6–10], which necessitates frequent measurements of the quantum system. Since existing experimental measurements are relatively slow and can degrade subsequent gate fidelities, such closed-loop optimization has yet to become practical for near-

* yzniu@mit.edu

† boixo@google.com

‡ smelyan@google.com

§ neven@google.com

term devices. The majority of open-loop control optimizations [11–13] address robustness through the analysis of the control noise spectrum and control curvature given by the control Hessian, which quickly becomes computationally exorbitant for multi-qubit-system control optimization as system size increases.

Undesirable couplings between a quantum computing system and its environment also become inevitable when the system is sufficiently large, which induces information leakage. Such leakage errors prevent the implementation of fast and high-fidelity quantum gates in many platforms such as superconducting qubits. Broadly speaking, two kinds of leakage abound: coherent leakage, which is deterministic and reversible in nature, caused by direct couplings between the qubit subspace and higher energy subspaces; and ‘incoherent leakage’, caused by either non-adiabatic transitions¹ during the modulation of system Hamiltonians or by photon loss to the environment. Coherent leakage can be further divided into on-resonant and off-resonant components, depending on whether the frequency components of the control are close to the energy gap separating the qubit subspace from a higher energy subspace (on-resonant) or not (off-resonant).

The structure of high-dimensional control landscapes of multi-qubit-system quantum control problems in the presence of leakage and control errors are poorly understood due to the lack of analytic tools and the prohibitive computational cost of numerical approaches. Despite this lack of precise knowledge of the control landscape, un-supervised machine learning techniques are able to obtain high-quality and scalable solutions to similar high-dimensional continuous-variable optimization in real-world problems. Notably, reinforcement learning (RL) stands out for its usefulness in the absence of labeled data because of its stability against sample noise and its effectiveness in the face of uncertainty and the stochastic nature of underlying physical systems. In RL, a software agent takes sequential actions aiming to maximize a reward function, or a negative cost function, that embodies the target problem. Successful training of an RL agent depends on balancing exploration of unknown territory with exploitation of existing knowledge.

Deep RL techniques [14–16] have revolutionized un-supervised machine learning through novel algorithm

designs which provide scalable, data efficient, and robust performance with an improvement guarantee. Further empowered by advanced optimization techniques using deep neural networks, they are able to solve more difficult high-dimensional optimization problems beyond the reach of classic RL techniques in benchmark tasks such as simulated robotic locomotion and Atari games [14–16]. While a classic RL technique, Q-learning, has been applied to quantum control problems recently [17, 18], these studies have not yet included practical leakage or control errors. We discover in this work that deep RL techniques are capable of solving more complex quantum control problems than previously attempted. The key to leveraging these advanced RL methods is to find an analytic cost function that incorporates the complete objective of the quantum optimization problem.

A comprehensive and efficiently computable leakage bound of the given control scheme is one missing piece of a universal control cost function to permit control optimization for any target unitary gate. Such lack of an explicit leakage bound also limits the generality of existing studies. For example, Refs. [19–22] study quantum controls over all independent single-qubit Hamiltonians to achieve a provably minimal gate time, but only for closed systems without leakage. To minimize on-resonant leakage errors, Ref. [23] turns off independent controls over the single-qubit Pauli Z couplings, and Refs. [1, 24, 25] turn off single-qubit Pauli X and Y couplings. These hard constraints, however, could impair the universality, or the controllability, over the quantum system: a time-dependent evolution without controls over *all* independent single-qubit Hamiltonians is no longer sufficient to implement an arbitrary unitary gate [19–21].

We propose a control framework, called Universal cost Function control Optimization (UFO), to overcome these fundamental challenges in quantum control by connecting deeper physical knowledge of the underlying quantum dynamics with state-of-the-art RL techniques. Instead of resorting from experimental randomized benchmarking for leakage quantification [26], we derive an analytic leakage bound for a Hamiltonian control trajectory to account for both on- and off-resonant leakage errors. Our leakage bound is based on a perturbation theory within the time-dependent Schrieffer-Wolff transformation (TSWT) formalism [27] and on a generalized adiabatic theorem, see App. B 1. The use of TSWT is a higher-order generalization of the derivative canceling method for adiabatic gates [28], where unwanted leakage errors are suppressed to any desired order by adding con-

¹ The non-adiabatic transition away from the qubit subspace results from the coherent quantum evolution of the full system, but in the context of the current study such transition is effectively incoherent since the transition back does not have time to occur.

control Hamiltonians proportional to associated orders of time-derivatives of the dominant system Hamiltonian. We relax hard constraints in control optimization to soft ones in the form of adjustable penalty terms of the cost function, offering more flexibility to an RL agent’s control policy while minimizing the meaningful errors from practical non-idealities. Our universal cost function enables a joint optimization over the accumulated leakage errors, violations of control boundary conditions, total gate time, and gate fidelity. Such a framework facilitates time-dependent controls over *all* independent single-qubit Hamiltonians and two-qubit Hamiltonians, thus achieving full controllability [19–21].

We use the UFO cost function as a reward for a continuous-variable policy-gradient RL agent, which is trained by trusted-region policy optimization [14], to find highest-reward/minimum-cost analog controls for a variety of two-qubit unitary gates. We find that applying second order gradient methods to a policy is superior to simpler approaches like direct gradient descent or differential evolution of the control scheme. We suspect this lies in its ability to leverage non-local features of control trajectories, which becomes crucial when the control landscape is high-dimensional and packed with a combinatorially large number of imperfect saddle points or local optima with vanishing gradients [29], which is often the case for open quantum systems [18]. Moreover, the calculation of control Hessians is replaced with a model-free second-order method with neural networks to further speed up the optimization process. In comparison, direct gradient descent methods are known to be incapable of rapidly escaping such high-dimensional saddle points [29].

Our RL agent comprises two neural networks (NN): one maps a given state containing the information about the simulated unitary gate at the current step to the probability distribution of proposed control actions for the next step (the policy NN); the other maps the same state to the projection of the discounted total future reward (the value function NN) [14]. Both NNs are fully connected with three layers of dimension 64, 32 and 32 respectively. Intuitively, the policy NN encodes the non-local regularities of numerous effective control solutions. Such regularities, traditionally captured by a carefully chosen analytic functional basis [13], are now represented by a model-independent NN without any prior knowledge of the mathematical structure of the target cost function. The value NN encodes the projected future interactions with a stochastic environment and the associated control cost, which is used to adjust the learning rate of the gradient descent of the policy

NN.

Both NNs of the RL agent interact with a training environment that evaluates the quantum dynamics under a given control action proposed by the RL agent and returns the updated unitary gate and the corresponding control cost (as reward); see Fig. 1. Optimization consists of many episodes, each of which contains all the time steps of a complete quantum control trajectory. The length of such a sampled control trajectory is determined by the minimum of a predefined runtime upper bound and the time it takes to meet a termination condition. In our case, the termination condition is measured by a satisfiable value of the UFO cost function. After sampling a batch of size 20000 many different episodes, the policy NN is updated to maximize the expected discounted future reward based on the proposed policy variation within the trusted region, and the value NN is updated to fit the expected discounted future reward based on the newly added samples. A detailed algorithm is presented in [14]. We discover that the robustness against control errors is significantly improved by simulating experimentally relevant Gaussian-random fluctuations in control amplitudes through a stochastic RL training environment.

We verify the quality and the robustness of our control scheme by evaluating the average fidelity of the noise-optimized control solution under different control noise model parameters. We compare the performance of our RL optimized control solution with the optimal gate synthesis. The latter provides the minimum number of required gates from a finite universal gate set for realizing the same unitary transformation. Our RL control solutions achieve up to a one-order-of-magnitude of improvement in gate time over the optimal gate synthesis approach based on the best known experimental gate parameters in superconducting qubits; an order of magnitude reduction in fidelity variance over solutions from both the noise-free RL counterpart and a baseline SGD method, and around two orders of magnitude reduction in average infidelity over control solutions from the SGD method.

In the perturbative regime, the gmon Hamiltonian consists of one-body and nearest-neighbor-two-body terms represented by bosonic creation and annihilation operators, \hat{a}_j^\dagger and \hat{a}_j , and bosonic number operators \hat{n}_j , for each j -th bosonic mode. In the rotating-wave approximation (RWA), with a constant rotation rate chosen as the harmonic frequency of the Josephson junction resonator (see App. A), the two-qubit gmon

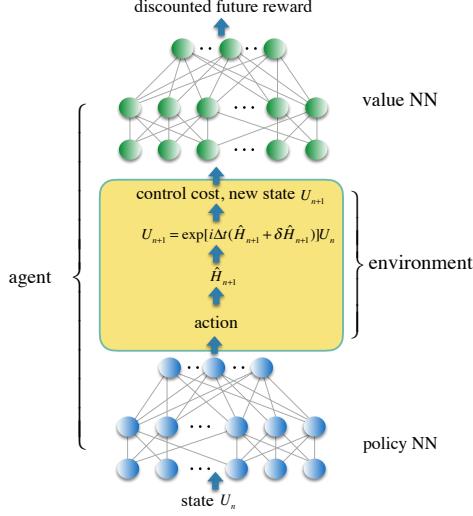


FIG. 1. Overview of the RL implementation: at the iteration time step $n+1$, the policy NN proposes a control action in the form of the system Hamiltonian \hat{H}_{n+1} , the training environment takes the proposed action and evaluates the Schrödinger equation under a noisy implementation $\hat{H}_{n+1} + \delta\hat{H}_{n+1}$ for time duration Δt to obtain a new unitary gate U_{n+1} and calculates the associated cost function, both of which are fed into an RL agent. The policy NN and value NN of the RL agent are updated jointly based on the trajectory of the simulated unitary gate, control action and associated control cost [30].

Hamiltonian takes the form:

$$\begin{aligned} \hat{H}_{\text{RWA}}(t) &= \frac{\eta}{2} \sum_{j=1}^2 \hat{n}_j(\hat{n}_j - 1) + g(t)(\hat{a}_2^\dagger \hat{a}_1 + \hat{a}_1^\dagger \hat{a}_2) \\ &+ \sum_{j=1}^2 \delta_j(t) \hat{n}_j + \sum_{j=1}^2 i f_j(t) \left(\hat{a}_j e^{-i\phi_j(t)} - \hat{a}_j^\dagger e^{i\phi_j(t)} \right), \end{aligned} \quad (1)$$

where the time-independent parameter η represents the anharmonicity of the Josephson junction, and the seven time-dependent control parameters are: amplitude $f_j(t)$ and phase $\phi_j(t)$ of the microwave control pulse, qubit detuning $\delta_j(t)$ with $j \in \{1, 2\}$, and tunable capacitive coupling or g-pulse $g(t)$. The computational subspace is spanned by the two lowest energy levels of each bosonic mode: $\mathcal{H}_2 = \text{Span}\{|0\rangle_j, |1\rangle_j\}$, where $|n\rangle_j$ represents a Fock state with n excitations in the j -th mode.

LEAKAGE ERROR BOUND

To identify different sources of leakage errors, we decompose Eq. (1) into three parts: $\hat{H}_{\text{RWA}}(t) = \hat{H}_0 + \hat{H}_1(t) + \hat{H}_2(t)$, where $\hat{H}_0 = \eta/2 \sum_{j=1}^2 \hat{n}_j(\hat{n}_j - 1)$ accounts for the large constant energy gaps separating the qubit subspace from other higher energy subspaces which also determines the minimum energy gap separating the qubit subspace from the nearest higher energy subspace denoted Δ , the block-diagonal Hamiltonian

$$\begin{aligned} \hat{H}_1(t) &= \sum_{j=1}^2 \delta_j(t) \hat{n}_j \\ &+ i f_1(t) \left(|0\rangle_1 \langle 1|_1 e^{-i\phi_1(t)} - |1\rangle_1 \langle 0|_1 e^{i\phi_1(t)} \right) \otimes \mathbb{I}_2 \\ &+ i f_2(t) \mathbb{I}_1 \otimes \left(|0\rangle_2 \langle 1|_2 e^{-i\phi_2(t)} - |1\rangle_2 \langle 0|_2 e^{i\phi_2(t)} \right) \\ &+ g(t) \left(|1\rangle_1 |0\rangle_2 \langle 1|_2 \langle 0|_1 + |0\rangle_1 |1\rangle_2 \langle 0|_2 \langle 1|_1 + h.c. \right) \\ &+ g(t) \left(|2\rangle_1 |1\rangle_2 \langle 2|_2 \langle 1|_1 + |1\rangle_1 |2\rangle_2 \langle 1|_2 \langle 2|_1 + h.c. \right) \end{aligned} \quad (2)$$

accounts for the coupling within the qubit subspace $\Omega_0 = \text{Span}\{|00\rangle, |10\rangle, |01\rangle, |11\rangle\}$ and within the first excited energy subspace $\Omega_1 = \text{Span}\{|20\rangle, |21\rangle, |12\rangle, |02\rangle\}$, and the block-off-diagonal $\hat{H}_2(t) = \hat{H}_{\text{RWA}}(t) - \hat{H}_0 - \hat{H}_1(t)$ accounts for the couplings between different energy subspaces with each other. It is the culprit behind leakage errors, but since both $\hat{H}_1(t)$ and $\hat{H}_2(t)$ derive from microwave pulses and the g-pulse, one cannot turn off $\hat{H}_2(t)$ without turning off controls over single-qubit Pauli X and Y from \hat{H}_1 which are otherwise crucial for obtaining the full controllability of the qubit system.

In order to suppress and evaluate coherent leakage errors induced by \hat{H}_2 , we adopt a rotated basis given by the TSWT framework, under the assumption that inter-subspace and intra-subspace couplings are much smaller than the energy gap separating different subspaces: $|f_j(t)| \sim |\delta_j(t)| \sim |g(t)| \sim \epsilon \ll \eta \sim \Delta$, see App. B 1. We use ϵ and Δ to denote the energy scale of the inter/intra subspace coupling strength and the large energy gap separating different energy subspaces, satisfying $\epsilon/\Delta \ll 1$. The effective block-off-diagonal Hamiltonian $\hat{\mathbb{H}}_{\text{od}}$ after the TSWT can thus be suppressed to any given higher order by applying the correct order of TSWT.

There are two independent sources of leakage errors for TSWT based quantum control that dominate in superconducting qubit gate controls: the first is the direct coupling leakage caused by the non-zero block-off-diagonal Hamiltonian after the second order TSWT,

and the second is the leakage caused by the violation of the adiabaticity due to the fast modulation of the system Hamiltonian. We derive in App. B 2 the bound for the coherent leakage errors as

$$L_{tot} = \frac{\|\hat{\mathbb{H}}_{od}(0)\|}{\Delta(0)} + \frac{\|\hat{\mathbb{H}}_{od}(t)\|}{\Delta(t)} + \int_0^t \frac{1}{\Delta^2(t)} \left\| \frac{d^2 \hat{\mathbb{H}}_{od}(t)}{dt^2} \right\| dt, \quad (3)$$

where $\hat{\mathbb{H}}_{od}$ represents the block-off-diagonal Hamiltonian, which is of magnitude $O(\frac{\epsilon^3}{\Delta^2})$ after the second order TSWT.

In addition to the coherent leakage errors bounded by Eq. (3) there also exists incoherent leakage errors due to the violation of adiabaticity from the time-dependent nature of our control quantum dynamics in the off-resonant regime. We derive a generalized adiabatic theorem to bound the non-adiabatic leakage error; see App.B 2. We show that such non-adiabatic leakage is not dominated in off-resonant frequency regime and Eq. (3) accounts for dominant leakage errors in both on-resonant and off-resonant regimes.

UNIVERSAL COST FUNCTION

An effective control cost function is crucial to an efficient control optimization and to guaranteeing the full controllability over the quantum system. We propose a control cost function that includes leakage errors, control constraints, total runtime, and gate infidelity as soft penalty terms that are readily optimizable using RL techniques without compromising the system controllability. We illustrate the design of a UFO cost function in the tunable gmon superconducting-qubit architecture [31].

A unitary gate is realizable through the control of the time-dependent Hamiltonian defined in Eq. (1) according to $U(T) = \mathbb{T}[\exp(-i \int_0^T \hat{H}_{RWA}(t) dt)]$, with \mathbb{T} denoting the time-ordering operator. The inaccuracy of the controlled two-qubit unitary gate $U(T)$ with respect to a target unitary gate U_{target} is measured by the gate infidelity: $1 - F[U(T)] = 1 - 1/16 |\text{Tr}(U^\dagger(T)U_{target})|^2$ [19–22], which vanishes only when $U(T) = U_{target}$ up to a global phase. This definition of control inaccuracy is widely used in quantum control optimization [1, 18–21, 24, 25, 28] for its little accompanying computational overhead during iterative optimizations. Gate infidelity can also be bounded

by the average gate infidelity measured through experimental benchmarking: lower gate infidelity implies lower average gate infidelity [32]. For these two reasons, we choose gate infidelity as the first part of our UFO cost function to penalize the control inaccuracy. The second part is a penalty term on the accumulated leakage errors derived above. The last two terms of the control cost function penalize the total runtime T and the violation of control boundary conditions. Boundary conditions are chosen to facilitate convenient gate concatenations: microwave pulses and the g-pulse should vanish at both boundaries such that the computational bases and the Fock bases coincide. This is enforced by adding $\sum_{t \in \{0, T\}} [g(t)^2 + f(t)^2]$ to the control cost function. Such boundary constraints also help to minimize the errors caused by deviations from RWA due to the fast oscillating nature of the non-RWA terms; see App. A. We thus obtain the full UFO cost function:

$$C(\chi, \beta, \gamma, \kappa) = \chi[1 - F[U(T)]] + \beta L_{tot} + \mu \sum_{t \in \{0, T\}} [g(t)^2 + f(t)^2] + \kappa T \quad (4)$$

where χ penalizes the gate infidelity, β penalizes different sources of leakage errors, μ penalizes the violation of boundary constraints, and κ penalizes the total runtime. These hyper-parameters are optimized to balance the joint optimization for achieving satisfactory control outcomes. To apply to other quantum computing platform where our control constraints no longer applies, each term of the UFO cost function can be modified to best describe optimization target based on the underlying physics.

TWO-QUBIT GATE CONTROL OPTIMIZATION

We now apply the UFO framework to find fast and high-fidelity two-qubit gate controls that are robust against control errors. We define the robustness of a gate control under a given control noise model as a bounded deviation of the average quantum gate fidelity $\bar{F}(\mathcal{E}, U_{target})$ from an ideal average gate fidelity F_{ideal} :

$$|\bar{F}(\mathcal{E}, U_{target}) - F_{ideal}| < \epsilon_0, \text{ for } \epsilon_0 > 0, \quad (5)$$

where

$$\bar{F}(\mathcal{E}, U_{target}) = \int d\psi \langle \psi | U_{target}^\dagger \mathcal{E}(|\psi\rangle\langle\psi|) U_{target} | \psi \rangle \quad (6)$$

embodies the quality of the gate-control quantum channel by averaging over the whole state space under a uniform Haar measure[33], with the trace-preserving quantum operation \mathcal{E} accounting for the noisy implementation of a target unitary U_{target} ; (see App. D). The average gate infidelity is defined accordingly as $1 - \bar{F}(\mathcal{E}, U)$.

Such a robustness criterion can be validated for a given control scheme using a number of computational steps that is linear in the total degrees of freedom of control parameters. However, it differs from the canonical definition in optimal control theory [11, 12], where the number of computational steps for the analysis of robustness using control Hessians scales cubically with the total degrees of freedom in control parameters. For special cases, such as closed-system single-qubit control, there exist analytic expressions for the control Hessian [11, 12]. But in the current work we choose a more practical definition of robustness scalable to multi-qubit control problems.

Traditional quantum control trajectory optimization depends on the complete knowledge of the underlying physical model. In contrast, the success and robustness of RL persist with incomplete and potentially flawed modeling. It is often the case in experiments that the exact control error model is unknown. Given partial information about the control error model, can we leverage RL optimization to find robust control solutions against not just one but a set of control error models? In our case, we deploy RL agents trained by trust-region policy optimization [14] in the OpenAI platform [34], to find near-optimal control solutions to the UFO cost function described in Eq. (4). We incorporate a pertinent control noise model of gmon superconducting-qubit Hamiltonian [31] into a stochastic training environment. At each time step, amplitude fluctuations sampled from a zero mean Gaussian distribution with 1 MHz variance, which amounts to around 5% control parameter uncertainty, are added to Hamiltonian parameters that are known to be prone to fluctuations: qubit anharmonicity, qubit detuning amplitudes, microwave control amplitudes and qubit g-pulse amplitude, see App. A. Harnessing the sample-noise resilience of RL optimization, we expect the optimized control to be robust against a family of control noise models despite being trained under a single model. This is indeed proven to be the case as evidenced by our numerical simulations.

$$\mathcal{N}(\alpha, \alpha, \gamma) = \exp[i(\alpha\sigma_1^x\sigma_2^x + \alpha\sigma_1^y\sigma_2^y + \gamma\sigma_1^z\sigma_2^z)] \quad (7)$$

In gmon superconducting qubits, the energy gap that

separates the qubit subspace from the nearest higher energy subspace is $\Delta(s) \approx 200$ MHz. We apply control frequency filters (App. C) to piece-wise constant analog control signals such that the frequency bandwidth of the proposed Hamiltonian modulation is limited to be within 10 MHz. Given that our off-diagonal Hamiltonian after the second order TSWT is of order 1/10 MHz (App. B 1), the first term of the leakage bound in Eq. (3), $\int_0^1 \frac{1}{\Delta^2(s)} \frac{1}{T} \left\| \frac{d^2 \hat{H}_{\text{od}}(s)}{ds^2} \right\| ds$, is of order 10^{-4} , around the fault-tolerant threshold value for leakage error of near-term surface code [35]. Although the gmon Hamiltonian is fully controllable under our UFO paradigm, we target at a family of two-qubit gates parametrized by $\mathcal{N}(\alpha, \alpha, \gamma) = \exp[i(\alpha\sigma_1^x\sigma_2^x + \alpha\sigma_1^y\sigma_2^y + \gamma\sigma_1^z\sigma_2^z)]$, where σ_j^k is the $k \in \{X, Y, Z\}$ Pauli matrix of the j -th qubit. The optimal gate synthesis [36] that provides the optimal decomposition of such unitary transformation into a minimum number of arbitrary single-qubit rotations and CZ gates corresponds to a depth seven circuit containing three two-qubit gates and five single-qubit gates, see Fig. 2. This gate family includes the SWAP, ISWAP, CNOT and CZ, fermionic swap gate, and Given's rotation up to single-qubit rotations. Both the fermionic swap gate and Given's rotations are used for realizing Jordan-Wigner transformations in fermionic Hamiltonian simulation [37–39]. Identifying continuous controls that outperform their optimal gate synthesis counterparts for this family of gates thus has far-reaching applications across quantum chemistry and quantum simulation. The hyper-parameters of the UFO cost function are optimized through a grid search and is applicable to all target gates we have considered: $\chi = \beta = 10, \mu = 0.2, \kappa = 0.1$.

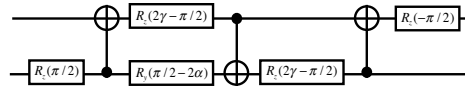


FIG. 2. Optimal gate synthesis for realizing unitary gate $\mathcal{N}(\alpha, \alpha, \gamma)$.

We compare our noise-optimized control obtained by the RL agent with the optimal gate synthesis counterpart in overall runtime. Based on state-of-the-art experimental implementations, we set the gate time for each single-qubit gate to 20ns and CNOT to 45ns. The optimal gate synthesis in Fig. 2 thus takes 215ns in runtime.

The gate times of our noise-optimized control schemes for three different values of γ are shown in

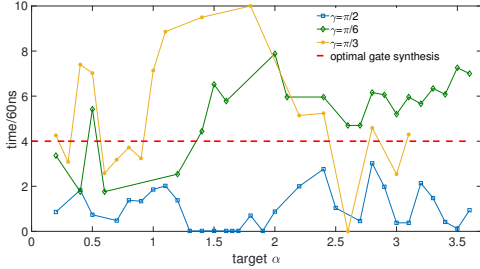


FIG. 3. Gate run time of two-qubit gate family $\mathcal{N}(\alpha, \alpha, \gamma)$ for $\gamma = \pi/2$ (blue curve), $\gamma = \pi/6$ (green curve) and $\gamma = \pi/3$ (yellow curve). The standard optimal gate synthesis run time for this gate family is around 200ns marked by dashed red line. Total leakage errors and gate infidelity are upper bounded by $O(10^{-4})$ and $O(10^{-3})$ respectively for all cases.

Fig. 3. There, different data points of the same γ are obtained by the same RL agent with an adaptive step size in α to guarantee a constant upper bound on the total optimization time: target gate α will be increased by one step $\alpha = \alpha + 0.1$, either when the agent obtains a control solution with a low enough overall cost, or when the optimization time for a given α exceeds a pre-defined value. We discover that it takes significantly less time for an RL agent to learn a new target unitary gate based on the successful learning of a nearby target than to learn a new target gate afresh, which provides heuristic evidence for the transfer learning facilitated by RL using deep NN².

We have seen a factor of 10 runtime improvement for the two-qubit gate family parametrized by $\mathcal{N}(\alpha, \alpha, \pi/2)$ with $\alpha \in [0, \pi]$ over the optimal gate synthesis. Such significant improvement manifests the hardware efficiency of our control optimization: the target unitary gate can be rewritten as $\mathcal{N}(\alpha, \alpha, \pi/2) = -\exp[i(\alpha\sigma_1^x\sigma_2^x + \alpha\sigma_1^y\sigma_2^y)]\exp[-i\frac{\pi}{2}\sigma_1^z]\exp[-i\frac{\pi}{2}\sigma_2^z]$ whose two-qubit entangling part is directly realizable through a time evolution under the gmon Hamiltonian defined in Eq. (1) without detuning or microwave controls: $\delta_j(t) = f_j(t) = 0$ with $j \in \{1, 2\}$. Our RL control optimization is thus able to detect such an inherent regularity, which relates a given system Hamiltonian to the family of target unitary gates that are efficiently

implementable. Isolated peaks in the gate time plot in Fig. 3 are potentially due to control singularities, which suggests the need for further studies into the hardness of the analog-control landscape in the presence of leakage and control errors.

We verify the robustness of the noise-optimized control solution \vec{c} from RL by evaluating its average fidelity $\bar{F}(\mathcal{E}, U_{\text{target}})$ and the variance of the control gate fidelities $F[U(\vec{c})]$ under different control noise instances $\delta\vec{c}$ sampled from the same Gaussian distribution $N(0, \sigma_{\text{noise}})$:

$$\sigma_{\text{fidelity}} = \mathbb{E}_{\delta\vec{c} \sim N(0, \sigma_{\text{noise}})} (F[U(\vec{c} + \delta\vec{c})] - F_{\text{ave}})^2, \quad (8)$$

$$F_{\text{ave}} = \mathbb{E}_{\delta\vec{c} \sim N(0, \sigma_{\text{noise}})} F[U(\vec{c} + \delta\vec{c})]. \quad (9)$$

We consider a Gaussian family of stochastic control error models: the amplitude fluctuations of control parameters are described by Gaussian distributions of zero mean and a variance σ_{noise} ranging from 0.1 MHz to 3.5 MHz. The gate control performance under the noise model with 1 MHz variance is a reasonable indicator for experimental implementations. Nevertheless, the exact value of control amplitude variance is hard to determine and can drift over time. The blue curve in Fig. 4 represents the average fidelity of the noise-optimized control by RL, which stays within the range of [99.5%, 98%] under the given noise model parameter range, satisfying our control robustness definition with $\epsilon_0 = 0.007$ at $\sigma_{\text{noise}} = 1\text{MHz}$. In Fig. 4, we compare noise-optimized control with a noise-free control solution obtained by an RL agent without a stochastic environment, represented by the green curve marked by diamonds, and with that obtained by a baseline stochastic gradient descent (SGD) technique using the Adam optimizer [40], represented by the red dashed lines. The noise-optimized control solution manifests up to a one-order-of-magnitude improvement in average gate infidelity over the noise-free control solution using RL, and around two-order-of-magnitude improvement in average gate infidelity over SGD baseline solutions. Moreover, the sampled fidelity variance of the noise-optimized RL solver is one order of magnitude lower than two other methods consistently throughout the tested noise model parameter range. This validates the improved stability of our control solution obtained by a policy-gradient trained RL agent against experimentally relevant Gaussian control noise models.

² The use of adaptive step size can be replaced by parallel RL agents, each dedicated to a fixed target unitary gate, which is not the focus of the current study.

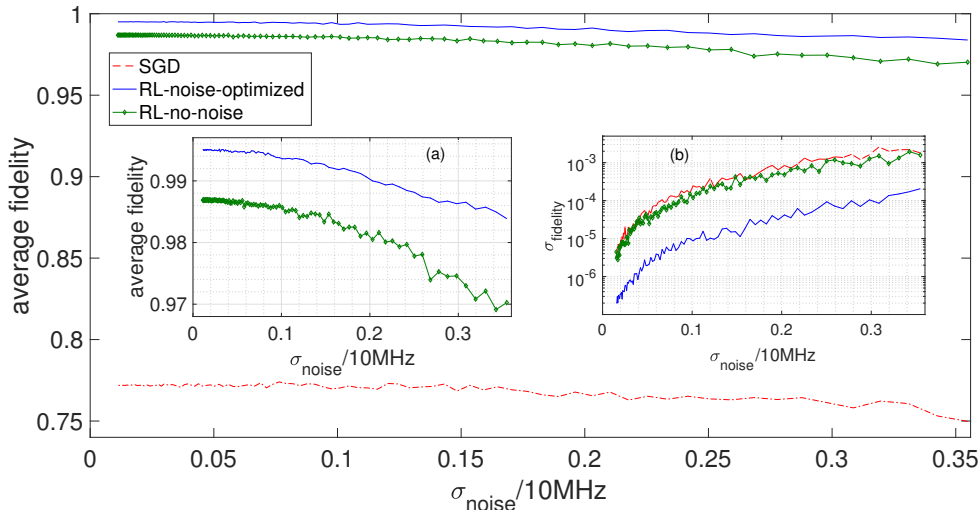


FIG. 4. Average fidelities of the optimized quantum control schemes vs the Gaussian control noise variance for the gate $\mathcal{N}(2.2, 2.2, \pi/2)$. The blue line represents the performance of the noise-optimized control obtained by an RL agent trained under a noisy environment. The green line marked by diamond shapes represents the performance of the control obtained by an RL agent with a noise-free environment. The red dashed line represents the performance of the control trajectory obtained by SGD. Subplot (a): zoomed in comparison of the average fidelities of the noise-optimized and noise-free RL control solutions under different values of Gaussian control noise variance. Subplot (b): comparison of fidelity variances of three different control schemes under different control noise variances σ_{noise} , where each data point is taken from 60 different control trajectories with control amplitude error at every time step sampled from the Gaussian distribution $\mathcal{N}(0, \sigma_{\text{noise}})$.

CONCLUSION

We propose a quantum control framework, UFO, for fast and high-fidelity quantum gate control optimization. It is applied to an open-loop control optimization through reinforcement learning, where the control trajectory is encoded by a first neural network (NN) and the control cost function is encoded by a second NN. Robust control solutions are obtained by training both NNs under a stochastic environment mimicking noisy control actuation. We achieve up to one order of magnitude reduction in average gate infidelity over noise-free alternatives and up to a one-order-of-magnitude reduction in gate time over the optimal gate synthesis solution. This is significant, given that the highest gate fidelity in state-of-the-art superconducting-qubit systems is around 99.5%, and that the total computation runtime is limited by decoherence to several microseconds.

Our work opens a new direction of quantum analog control optimization using RL, where unpredictable control errors and incomplete physical models of environmental interactions are taken into account dur-

ing the control optimization. Other advanced machine learning techniques are also readily applicable to our control framework. The success of deep RL in Alpha Go [16] and robotic control [14, 15] suggests that our approach—once generalized to closed-loop control optimization, where system calibration and gate control optimization are combined into a unified procedure—could further improve control robustness towards systematic and time-correlated errors.

Acknowledgement We thank Charles Neil and Pedram Roushan for helpful discussions on the experimental noise models and detailed control parameters in the gmon superconducting qubit implementation. M. Y. N. thanks Barry C. Sanders for early discussions on control optimization through reinforcement learning, Isaac L. Chuang for useful comments on the draft, Théophane Weber, Martin McCormick and Lucas Beyer for discussions on reinforcement learning methods. M. Y. N. acknowledges financial support from the Google research internship summer 2017 program during which the majority of the work was performed. M. Y. N. acknowledges support from the Claude E. Shannon Research Assistantship.

Author Contributions. M. Y. N, S. B. and V. S. developed the project and theory. M. Y. N. implemented the reinforcement algorithms and numerical studies. All authors contributed to the draft.

Appendix A: Gmon Hamiltonian and Control Noise

We focus on the two-qubit gmon Hamiltonian in the perturbative regime as an example. It is obtained by quantizing a phenomenological classical Hamiltonian for non-linear L-C circuits containing Josephson junctions, as explained below.

1. Quantum Oscillator Picture

The supercurrent across a Josephson junction between two superconducting media, in the absence of any external field, persists and undergoes quantum oscillations once connected to a capacitor. Intuitively, it is the quantum tunneling across the junction that drives the supercurrent. Such macroscopic quantum effect is associated with a phenomenological classical circuit model, where the effective voltage across the Josephson junction comes from the changing of the phase difference ϕ across the junction as

$$V = \frac{\phi_0}{2\pi} \frac{d\phi}{dt}, \quad (\text{A1})$$

where $\phi_0 = h/2e$ and e is the electron charge. Moreover, the supercurrent depends on the phase difference as

$$I = I_c \sin(\phi), \quad (\text{A2})$$

where the critical current I_c is a parameter characterizing the junction. Once we connect it to a capacitor of capacitance C , we obtain a nonlinear quantum oscillation. We write the potential energy of the inductor as

$$U = \int IV dt = \frac{\phi_0 I_c}{2\pi} \int \sin(\phi) \frac{d\phi}{dt} dt = -E_J \cos \phi. \quad (\text{A3})$$

The energy contribution from the capacitor

$$T = \frac{1}{2} CV^2 = \frac{1}{2} C \left(\frac{\phi_0}{2\pi} \dot{\phi} \right)^2 \quad (\text{A4})$$

can be regarded as the kinetic term of the oscillator energy. The Hamiltonian for the Josephson junction oscillator, to lowest order in ϕ , is

$$H_0 = U_0 + T = \alpha \phi^2 + \beta \dot{\phi}^2, \quad (\text{A5})$$

with α and β determined by the effective capacitance and inductance of the superconducting circuit. For example, we can add additional inductor into the Josephson L-C circuit to change the potential energy of the effective inductance of the whole circuit.

To analyze the quantum dynamics of this phenomenological model derived from its classical analogue, we perform second quantization of ϕ by treating it as one of the two quadratures of a bosonic field:

$$\hat{\phi} = \kappa \frac{\hat{a}^\dagger + \hat{a}}{\sqrt{2}}, \quad (\text{A6})$$

where $\kappa = (\beta/\alpha)^{1/4}$. The conjugate basis $\hat{\dot{\phi}}$ takes the form

$$\hat{\dot{\phi}} = \kappa^{-1} \frac{\hat{a}^\dagger - \hat{a}}{\sqrt{2}i}. \quad (\text{A7})$$

Under this quantization, the harmonic part of the Josephson L-C circuit Hamiltonian is

$$\hat{H}_0 = \omega_0 \left(\hat{a}^\dagger \hat{a} + \frac{1}{2} \right), \quad (\text{A8})$$

where we have set $\hbar = 1$ and defined $\omega_0 = \sqrt{\kappa}$.

Now let us include the lowest order anharmonic term from Eq. (A3) to the Josephson L-C circuit Hamiltonian:

$$\hat{H}_1 = \gamma \hat{\phi}^4 = \frac{\gamma \kappa^4}{4} (\hat{a} + \hat{a}^\dagger)^4 \quad (\text{A9})$$

$$= \frac{\eta}{8} \left[(\hat{a}^2 + (\hat{a}^\dagger)^2)^2 + (\hat{a}^2 + (\hat{a}^\dagger)^2) (2\hat{n} + 1) + (2\hat{n} + 1) (\hat{a}^2 + (\hat{a}^\dagger)^2) + (2\hat{n} + 1)^2 \right] \quad (\text{A10})$$

with $\hat{n} = \hat{a}^\dagger \hat{a}$, γ determined by the configurations of additional inductor or capacitor elements added into the Josephson L-C circuit and η as a parametrization following literature convention.

The coupling between two qubits is realized by turning on the capacitive coupling between two Josephson L-C circuits. To the lowest order, such capacitive coupling energy depends on ϕ_1 and ϕ_2 as:

$$\hat{H}_2 = -\alpha'(t) \dot{\phi}_1 \dot{\phi}_2 = -\frac{\alpha'(t)}{2\kappa_1 \kappa_2} (\hat{a}_1^\dagger - \hat{a}_1) (\hat{a}_2^\dagger - \hat{a}_2), \quad (\text{A11})$$

where the capacitive coupling strength $\alpha'(t)$ is tunable.

Additionally, we also have capacitive coupling between a strong non-depleted microwave pulse and our quantized bosonic modes as

$$T_{\text{micro}} = \frac{1}{2} C V_{\text{drive}} V_{\text{qubit}}. \quad (\text{A12})$$

The microwave drive induced voltage is proportional to the field amplitude

$$V_{\text{drive}} = f(t) e^{-i\omega t - \phi} + f(t) e^{i\omega t + \phi} \quad (\text{A13})$$

with c-number $F(t)$ determined by the amplitude of the microwave drive, ϕ being the phase of the drive and ω being the frequency of the drive. The quantized voltage of the bosonic field, on the other hand, can be represented by the conjugate phase operator defined in Eq. (A7)

$$V_{\text{qubit}} = i(\hat{a}_j - \hat{a}_j^\dagger) \quad (\text{A14})$$

up to a real-valued constant factor. Putting together the voltage dependence on the control field and quantized bosonic modes, we obtain the microwave pulse controlled capacitive energy:

$$\hat{H}_3 = \sum_{j=1,2} i \left(\hat{a}_j - \hat{a}_j^\dagger \right) f_j(t) \cos(\omega_j t + \phi_j), \quad (\text{A15})$$

where ω_j , ϕ_j , and $f_j(t)$ represents respectively the frequency, phase and amplitude of each microwave pulse. The overall system Hamiltonian thus comprises four parts

$$\hat{H} = \hat{H}_0 + \hat{H}_1 + \hat{H}_2 + \hat{H}_3. \quad (\text{A16})$$

We further simplify this Hamiltonian by switching to the interaction picture

$$\hat{H}_I = U \left(\hat{H} - \hat{H}_0 \right) U^\dagger \quad (\text{A17})$$

with $U = e^{-i\hat{H}_0 t}$ and

$$\hat{H}_0 = (\bar{\omega}_0 + \eta) \hat{n} = \tilde{\omega}_0 \hat{n}. \quad (\text{A18})$$

The Hamiltonian for two bosonic modes hosted by two coupled gmon circuits in the interaction picture thus takes the form

$$\begin{aligned} \hat{H}_I = & \sum_{j=1}^2 \delta_j \hat{n}_j + \frac{\eta}{8} \sum_{j=1}^2 \left[\left(\hat{a}_j^2 e^{-2i\tilde{\omega}_0 t} + (\hat{a}_j^\dagger)^2 e^{2i\tilde{\omega}_0 t} \right)^2 + \left(\hat{a}_j^2 e^{-2i\tilde{\omega}_0 t} + (\hat{a}_j^\dagger)^2 e^{-2i\tilde{\omega}_0 t} \right) (2\hat{n}_j + 1) \right. \\ & + (2\hat{n}_j + 1) \left(\hat{a}_j^2 e^{-2i\tilde{\omega}_0 t} + (\hat{a}_j^\dagger)^2 e^{2i\tilde{\omega}_0 t} \right) + 4\hat{n}_j^2 - 4\hat{n}_j + 1 \Big] \\ & - \frac{\alpha'(t)}{2\kappa_1\kappa_2} (\hat{a}_1^\dagger \hat{a}_2^\dagger e^{2i\tilde{\omega}_0 t} + \hat{a}_1 \hat{a}_2 e^{-2i\tilde{\omega}_0 t} - \hat{a}_2^\dagger \hat{a}_1 - \hat{a}_1^\dagger \hat{a}_2) \\ & + \sum_{j=1,2} i \left(\hat{a}_j (e^{-i(\tilde{\omega}_0 + \omega_j)t - i\phi} + e^{-i(\tilde{\omega}_0 - \omega_j)t + i\phi}) - \hat{a}_j^\dagger (e^{i(\tilde{\omega}_0 + \omega_j)t + i\phi} + e^{i(\tilde{\omega}_0 - \omega_j)t - i\phi}) \right) f_j(t), \quad (\text{A19}) \end{aligned}$$

where $\delta_j = \tilde{\omega}_0 - \omega_0$ is the detuning of each qubit from the initial harmonic frequency. The simulation time of the gmon system t is usually set to be much longer than $1/\eta$ satisfying $t\tilde{\omega}_0 \gg 1$. We can therefore apply the rotating-wave-approximation (RWA) to omit the highly oscillating components with phase oscillating equal or faster than $\tilde{\omega}_0$. As a result, we obtain the Hamiltonian for the gmon circuit bosonic modes in RWA basis as

$$\hat{H}_{\text{RWA}} = \frac{\eta}{2} \sum_{j=1}^2 \hat{n}_j (\hat{n}_j - 1) + g(t) (\hat{a}_2^\dagger \hat{a}_1 + \hat{a}_1^\dagger \hat{a}_2) + \sum_{j=1}^2 \delta_j(t) \hat{n}_j + \sum_{j=1}^2 i f_j(t) \left(\hat{a}_j e^{i\phi_j(t)} - \hat{a}_j^\dagger e^{-i\phi_j(t)} \right), \quad (\text{A20})$$

where we assumed that the microwave frequencies ω_j are not too far from the qubit frequency $\tilde{\omega}_0$ such that $\Delta\omega = \tilde{\omega}_0 - \omega_j \ll \tilde{\omega}_0$, and define $g(t) = \alpha'(t) \frac{\kappa_1 \kappa_2}{2}$.

	η	$g(t)$	$\delta_j(t)$	$f_j(t)$	$\phi_j(t)$
amplitude	200 MHz	[-20, 20] MHz	[-20, 20] MHz	[-20, 20] MHz	[0, 2π]
error amplitude	± 1 MHz	± 1 MHz	± 1 MHz	± 1 MHz	

TABLE I. Hamiltonian control parameter range.

The above Hamiltonian describes the two coupled Josephson L-C circuits in the perturbative regime of the anharmonicity. The parameter range of its coupling terms are listed in Table. I. We require that the magnitudes of our two-qubit coupling g-pulse $g(t)$, detuning $\delta_j(t)$ and microwave pulse amplitude $f_j(t)$ are at least one magnitude lower than η to meet our leakage minimization condition. Moreover, we make the modulation rate of all parameters $g(t), \delta_j(t), f_j(t)$ to be within the frequency bandwidth $[-50, 50]$ MHz due to experimental limitations. Projected onto the qubit basis, this Hamiltonian takes the form:

$$\hat{H}_{\text{RWA}} = \frac{g(t)}{2} (\sigma_1^x \sigma_2^x + \sigma_1^y \sigma_2^y) \sum_{j=1}^2 \left[\frac{\delta_j(t)}{2} \sigma_j^z - f_j(t) (\sin \phi_j(t) \sigma_j^x + \cos \phi_j(t) \sigma_j^y) \right]. \quad (\text{A21})$$

The stochastic training environment is implemented by adding amplitude fluctuation sampled from a zero mean Gaussian distribution of 1 MHz variance to the six control amplitudes $\eta \rightarrow \eta + \delta\eta$, $g(t_k) \rightarrow g(t_k) + \delta g(t_k)$, $\delta_j(t_k) \rightarrow \delta_j(t_k) + \delta\delta_j(t_k)$ and $f_j(t_k) \rightarrow \delta f_j(t_k)$ in every discretized time step $t_k \in [0, \Delta T, 2\Delta T, \dots, N\Delta T]$.

Appendix B: Complete Leakage Bound

In the following sections, we focus on deriving the correct form of L_{tot} to fully account for different sources of leakage errors during a time-dependent Hamiltonian evolution. We start with the formulation of TSWT for defining a rotated computational basis, where direct coupling induced leakage errors are suppressed to the higher order. Next, we prove that the non-adiabatic leakage from our generalization of adiabatic theorem under TSWT is sub-dominant to obtain the final leakage bound L_{tot} defined in Eq. (9) of the main text.

1. Time-dependent Schrieffer-Wolff transformation

The success of Schrieffer-Wolff transformation [27] rests upon the difference in energy scales between the energy gap separating different subspaces and the coupling terms within and between different subspaces. To generalize the previous formulation, we decompose the system Hamiltonian into three parts

$$\hat{H}(t) = \hat{H}_0 + \hat{H}_1(t) + \hat{H}_2(t), \quad (\text{B1})$$

$$\hat{H}_0 = \sum_{\alpha} \sum_{m \in \Omega_{\alpha}} E_1 |m\rangle \langle m|, \quad (\text{B2})$$

$$\hat{H}_1(t) = \sum_{\alpha} \sum_{m \in \Omega_{\alpha}} \langle m | \hat{H}_1^{\alpha}(t) | m' \rangle |m\rangle \langle m'|$$

$$\hat{H}_2(t) = \sum_{\alpha \neq \alpha'} \sum_{m \in \Omega_{\alpha}, m' \in \Omega_{\alpha'}} \langle m | \hat{H}_2^{\alpha, \alpha'}(t) | m' \rangle | \alpha, m \rangle \langle \alpha', m' |,$$

where Ω_{α} with $\alpha \in \{0, 1, 2, \dots\}$ represents different subspaces and $|m\rangle$ denotes orthogonal basis state spanning each same subspace, the first term \hat{H}_0 accounts for the time-independent part of the system Hamiltonian, the second term $\hat{H}_1(t)$ accounts for the time-dependent coupling within each subspace Ω_{α} which we call the ‘‘block-diagonal term’’, and the third part $\hat{H}_2(t)$ accounts for the coupling between different subspaces which we call the ‘‘block-off-diagonal term’’. In order to apply the perturbative expansion of TSWT, we assume the magnitudes of three parts of the system Hamiltonian obey: $\Delta = \min_{\alpha \neq 0} |E_{\alpha} - E_0| \gg |\langle m | \hat{H}_1^{\alpha}(t) | m' \rangle| \sim |\langle m | \hat{H}_2^{\alpha, \alpha'}(t) | l \rangle| \epsilon$, for $\forall m, m' \in \Omega_{\alpha}, l \in \Omega_{\alpha'}, \alpha \neq \alpha'$ through out the time-dependent Hamiltonian evolution, where we use Δ and ϵ to represent the different energy scales satisfying $\epsilon/\Delta \ll 1$. Under this assumption, each subspace Ω_{α} is separated from the other by energy gap much larger than the coupling within Ω_{α} or between Ω_{α} and Ω_{β} for $\beta \neq \alpha$. Now we perform the Schrieffer-Wolff transformation to rotate the original basis state $|\psi\rangle$ to $|\tilde{\psi}\rangle = e^{-\hat{S}}|\psi\rangle$. In this rotated basis, the effective Hamiltonian $\hat{\mathbb{H}}$ can be found by

$$i \frac{d}{dt} |\tilde{\psi}\rangle = \hat{\mathbb{H}} |\tilde{\psi}\rangle = i \frac{d e^{-\hat{S}}}{dt} e^{\hat{S}} |\tilde{\psi}\rangle + i e^{-\hat{S}} \frac{d}{dt} |\psi\rangle, \quad (\text{B3})$$

$$\hat{\mathbb{H}} = -i \sum_{j=0}^{\infty} \frac{1}{(j+1)!} [\dot{\hat{S}}, \hat{S}]_j + e^{-\hat{S}} \hat{H} e^{\hat{S}}, \quad (\text{B4})$$

where the anti-Hermitian operator $\hat{S}(t)$ contains non-zero term only between different subspaces and is thus block-off-diagonal. The goal of TSWT is to find perturbative solution of the rotation $\hat{S}(t) = \epsilon \hat{S}_1(t) + \epsilon^2 \hat{S}_2(t) + \dots + \epsilon^n \hat{S}_n(t)$ that block-diagonalizes the system Hamiltonian [27] such that the effective Hamiltonian $\hat{\mathbb{H}}$'s block-off-diagonal terms are suppressed to an order of $O\left(\frac{\epsilon^{n+1}}{\Delta^n}\right)$ for n th order perturbative solution of $\hat{S}(t)$. We provide the derivation of $\hat{S}(t)$ up to the second order as a function of $\hat{H}(t)$ below.

We expand the expression for the effective Hamiltonian in Eq. (B4) into

$$\hat{\mathbb{H}} = -i \sum_{j=0}^{\infty} \frac{1}{(j+1)!} [\dot{\hat{S}}, \hat{S}]_j + \sum_{j=0}^{\infty} \frac{1}{j!} [\hat{H}(t), \hat{S}(t)]^j \quad (\text{B5})$$

using the algebraic relation

$$e^{-\hat{S}(t)} \hat{H}(t) e^{\hat{S}(t)} = \sum_{j=0}^{\infty} \frac{1}{j!} [\hat{H}(t), \hat{S}(t)]^j, \quad (\text{B6})$$

$$[\hat{H}(t), \hat{S}(t)]^j = [\dots [\hat{H}(t), \underbrace{\hat{S}(t), \hat{S}(t)}_{j \text{ many}}] \dots, \hat{S}(t)]. \quad (\text{B7})$$

We can now separate Eq. (B5) into block-diagonal and block-off-diagonal component and choose correct form of rotation $\hat{S}(t)$ to cancel the block-off-diagonal component to a given order. For simplicity, henceforth we do not write down the time-dependency (t) for each operator.

As defined in the main text, \hat{H}_0 and \hat{H}_1 are block-diagonal, while \hat{S} and \hat{H}_2 are block-off-diagonal. Therefore, even orders of the commutation in Eq. (B7) between \hat{H}_0 or \hat{H}_1 with \hat{S} or $\dot{\hat{S}}$ are block-diagonal, while their odd counterparts are block-off-diagonal. And the odd orders of commutations between \hat{H}_2 or $\dot{\hat{S}}$ with \hat{S} are block-diagonal and their odd counterparts are block-off-diagonal. We thus obtain block-diagonal part of Eq. (B6):

$$\hat{\mathbb{H}}_d = -i \sum_{j=0}^{\infty} \frac{1}{(2j+2)!} [\dot{\hat{S}}, \hat{S}]^{2j+1} + \sum_{j=0}^{\infty} \frac{1}{2j!} [\hat{H}_0 + \hat{H}_1, \hat{S}]^{2j} + \sum_{j=0}^{\infty} \frac{1}{(2j+1)!} [\hat{H}_2, \hat{S}]^{2j+1}. \quad (\text{B8})$$

Similarly we obtain the block-off-diagonal part of the effective Hamiltonian:

$$\hat{\mathbb{H}}_{\text{od}} = -i \sum_{j=0}^{\infty} \frac{1}{(2j+1)!} [\dot{\hat{S}}, \hat{S}]^{2j} + \sum_{j=0}^{\infty} \frac{1}{(2j+1)!} [\hat{H}_0 + \hat{H}_1, \hat{S}]^{2j+1} + \sum_{j=0}^{\infty} \frac{1}{2j!} [\hat{H}_2, \hat{S}]^{2j}. \quad (\text{B9})$$

Now we like to set the block-off-diagonal component to zero up to the order $O(\epsilon^3/\Delta^2)$. With a slight abuse of notation, we use below ϵ in short for the unitless value ϵ/Δ . We solve such diagonalization through perturbative expansion of the TSWT rotation: $\hat{S} = \epsilon \hat{S}_1 + \epsilon^2 \hat{S}_2 + \dots + \epsilon^n \hat{S}_n$ and $\dot{\hat{S}} = \epsilon^2 \dot{\hat{S}}_1 + \epsilon^3 \dot{\hat{S}}_2 + \dots + \epsilon^{n+1} \dot{\hat{S}}_n$ such that we solve order by order rotation $\hat{S}_n(t)$ that cancels the block-off-diagonal parts of the Hamiltonian of order $O(\epsilon^n)$.

Here, we adopt the convention that the time derivative of each order of rotation is one order higher: $|\dot{\hat{S}}_n| \sim \epsilon |\hat{S}|$.

Following the same convention, we rewrite the original Hamiltonian as $\hat{H} = \hat{H}_0 + \epsilon(\hat{H}_1 + \hat{H}_2)$ according to relative amplitudes of different components, and insert it together with expansion of $\hat{S}(t)$ to obtain the order by order perturbative expansion of block-diagonal and block-off-diagonal parts of the effective Hamiltonian:

$$\hat{\mathbb{H}}_d = \hat{H}_0 + \epsilon \hat{H}_1 + \frac{1}{2} \epsilon^2 [\hat{H}_2, \hat{S}_1] + \frac{1}{2} \epsilon^3 [\hat{H}_2, \hat{S}_2] - i \frac{1}{2} \epsilon^3 [\dot{\hat{S}}_1, \hat{S}_1] + O(\epsilon^4), \quad (\text{B10})$$

$$\begin{aligned} \hat{\mathbb{H}}_{\text{od}} = & \epsilon [\hat{H}_0, \hat{S}_1] + \epsilon \hat{H}_2 + \epsilon^2 [\hat{H}_0, \hat{S}_2] + \epsilon^2 [\hat{H}_1, \hat{S}_1] - i \epsilon^2 \dot{\hat{S}}_1 \\ & + \epsilon^3 [\hat{H}_1, \hat{S}_2] + \frac{\epsilon^3}{3} [[\hat{H}_2, \hat{S}_1], \hat{S}_1] - i \epsilon^3 \dot{\hat{S}}_2 + O(\epsilon^4). \end{aligned} \quad (\text{B11})$$

Perturbatively diagonalizing the Hamiltonian, to the first order in ϵ we have

$$[\hat{H}_0, \hat{S}_1] + \hat{H}_2 = 0, \quad (\text{B12})$$

which gives us the matrix expression for the first order SW rotation

$$\hat{S}_1^{\alpha, \alpha'} = \frac{\hat{H}_2^{\alpha, \alpha'}}{E_{\alpha'} - E_{\alpha}} \quad (\text{B13})$$

where $\hat{H}_2^{\alpha, \alpha'}$ is the Hamiltonian between subspace Ω_{α} and $\Omega_{\alpha'}$ and is itself a matrix. To the second order in diagonalization, we have

$$[\hat{H}_0, \hat{S}_2] + [\hat{H}_1, \hat{S}_1] - i \dot{\hat{S}}_1 = 0, \quad (\text{B14})$$

which immediately yields the matrix representation of the second order SW rotation between subspace Ω_{α} and Ω'_{α} :

$$\hat{S}_2^{\alpha, \alpha'} = \frac{\hat{H}_1^{\alpha} \hat{H}_2^{\alpha, \alpha'} - \hat{H}_2^{\alpha, \alpha'} \hat{H}_1^{\alpha'}}{(E_{\alpha'} - E_{\alpha})^2} - \frac{i \dot{\hat{H}}_2^{\alpha, \alpha'}}{(E_{\alpha'} - E_{\alpha})^2} \quad (\text{B15})$$

where we use \hat{H}_1^α as the sub-dominant Hamiltonian terms within the subspace Ω_α . Inserting Eq. (B13) and (B15) into Eq. (B10) and (B11) gives us the block-diagonal and block-off-diagonal parts of the effective Hamiltonian after the second order TSWT:

$$\begin{aligned}
(\hat{\mathbb{H}}_d)^\alpha &= \hat{H}_0^\alpha + \hat{H}_1^\alpha - \sum_{\alpha' \neq \alpha} \frac{\hat{H}_2^{\alpha, \alpha'} \hat{H}_2^{\alpha', \alpha}}{(E_{\alpha'} - E_\alpha)} \\
&+ \frac{1}{2} \sum_{\alpha' \neq \alpha} \frac{\hat{H}_2^{\alpha, \alpha'} \hat{H}_2^{\alpha', \alpha} \hat{H}_1^\alpha - \hat{H}_1^\alpha \hat{H}_2^{\alpha, \alpha'} \hat{H}_2^{\alpha', \alpha}}{(E_{\alpha'} - E_\alpha)^2} \\
&+ \sum_{\gamma \neq \alpha} i \left[\frac{\hat{H}_2^{\alpha, \gamma} \hat{H}_2^{\gamma, \alpha} - \hat{H}_2^{\alpha, \gamma} \hat{H}_2^{\gamma, \alpha}}{(E_\alpha - E_\gamma)^2} \right] + O(\epsilon^4), \\
(\hat{\mathbb{H}}_{od})^{\alpha, \alpha'} &= \hat{H}_{od}^{\alpha, \alpha'} + \Delta \hat{H}_{od}^{\alpha, \alpha'}, \\
&= \frac{(\hat{H}_1^\alpha)^2 \hat{H}_2^{\alpha, \alpha'} - 2 \hat{H}_1^\alpha \hat{H}_2^{\alpha, \alpha'} \hat{H}_1^{\alpha'} + \hat{H}_2^{\alpha, \alpha'} (\hat{H}_1^{\alpha'})^2}{(E_{\alpha'} - E_\alpha)^2} \\
&+ \frac{2}{3(E_{\alpha'} - E_\alpha)} \sum_\gamma \left[\frac{\hat{H}_2^{\alpha, \alpha'} \hat{H}_2^{\alpha', \gamma} \hat{H}_2^{\gamma, \alpha'}}{E_{\alpha'} - E_\gamma} - \frac{\hat{H}_2^{\alpha, \gamma} \hat{H}_2^{\gamma, \alpha} \hat{H}_2^{\alpha, \alpha'}}{E_\alpha - E_\gamma} \right] \\
&- i \left[\frac{\hat{H}_1^\alpha \hat{H}_2^{\alpha, \alpha'} + 2 \hat{H}_1^\alpha \hat{H}_2^{\alpha, \alpha'} - 2 \hat{H}_2^{\alpha, \alpha'} \hat{H}_1^{\alpha'} - \hat{H}_2^{\alpha, \alpha'} \hat{H}_1^{\alpha'}}{(E_{\alpha'} - E_\alpha)^2} \right] - \frac{\ddot{H}_2^{\alpha, \alpha'}}{(E_{\alpha'} - E_\alpha)^2} + O(\epsilon^4) \quad (\text{B17})
\end{aligned}$$

With this block-off-diagonal Hamiltonian in hand, we continue to evaluate the population leakage out of the qubit subspace caused by this direct coupling in both off-resonant and on-resonant regimes in the following section.

2. Leakage Bound

Direct Coupling Leakage Bound:

The non-zero block-off-diagonal part of the Hamiltonian $\hat{\mathbb{H}}_{od}$ directly couples the qubit subspace to the higher energy subspace. To evaluate the population that transition out of the qubit subspace due to this direct couplings, we adopt the interacting picture with state basis $|\psi(t)\rangle_I = U_d^{-1}(t)|\psi(t)\rangle$ that relates to the Schrödinger picture basis initial state $|\psi(0)\rangle$ by a block-diagonal Hamiltonian evolution $U_d(t) = \mathbb{T}[e^{-i \int_0^t \hat{\mathbb{H}}_d(\tau) d\tau}]$, where \mathbb{T} represents the time-ordering. The Schrödinger equation in the interacting picture is $i \frac{d}{dt} |\psi(t)\rangle_I = U_d^{-1}(t) \hat{\mathbb{H}}_{od}(t) U_d(t) |\psi(0)\rangle_I$ with the lowest order solution given $|\hat{\mathbb{H}}_{od}(t)\rangle_I$ is of order $O(\epsilon^3/\Delta^2)$:

$$|\psi(t)\rangle_I \approx \left[I - i \int_0^t U_d^{-1}(\tau) \hat{\mathbb{H}}_{od}(\tau) U_d(\tau) d\tau \right] |\psi(0)\rangle \quad (\text{B18})$$

where we insert the initial condition $|\psi(0)\rangle_I = |\psi(0)\rangle$. Since $U_d(t)$ preserve the computational subspace, the leakage is thus evaluated by the sum of the amplitudes of all excited states outside the qubit subspace due to the

non-zero block-off-diagonal Hamiltonian after TSWT:

$$\begin{aligned}
L_{\text{direct}}(t) &= \sum_{\alpha \neq 0, m \in \Omega_\alpha} |\langle m(t) | (U_d(0) |\psi(0)\rangle - U_d(t) |\psi(t)\rangle_I) | \\
&= \sum_{\alpha \neq 0, m \in \Omega_\alpha} \left| \langle m(t) | \int_0^t U_d(t, \tau) \hat{\mathbb{H}}_{\text{od}}(\tau) U_d(\tau, t) d\tau |\psi(t)\rangle \right| \\
&\stackrel{1}{\approx} \sum_{\alpha \neq 0, m \in \Omega_\alpha} \left| \langle m(t) | \left(U_d(t, \tau) \frac{1}{\Delta_\alpha} \hat{\mathbb{H}}_{\text{od}}(\tau) U_d(\tau, t) \right) \right|_{\tau=0}^t \\
&\quad - \left| \int_0^t U_d(t, \tau) \frac{1}{\Delta_\alpha} \frac{d}{d\tau} \left(\hat{\mathbb{H}}_{\text{od}}(\tau) \hat{\mathbb{H}}_{\text{d}}^{-1} \frac{dU_d(\tau, t)}{d\tau} \right) d\tau |\psi(t)\rangle \right| \\
&\stackrel{2}{=} \sum_{\alpha \neq 0, m \in \Omega_\alpha} \left| \langle m(t) | \left(U_d(t, \tau) \frac{1}{\Delta_\alpha} \hat{\mathbb{H}}_{\text{od}}(\tau) U_d(\tau, t) \right) \right|_{\tau=0}^t \\
&\quad - \left(2U_d(t, \tau) \frac{1}{\Delta_\alpha^2} \frac{d\hat{\mathbb{H}}_{\text{od}}(\tau)}{d\tau} \frac{dU_d(\tau, t)}{d\tau} \right) \Big|_{\tau=0}^t + \int_0^t U_d(t, \tau) \frac{1}{\Delta_\alpha^2} \frac{d^2 \hat{\mathbb{H}}_{\text{od}}(\tau)}{d\tau^2} U_d(\tau, t) |\psi(t)\rangle \Big| \\
&\stackrel{3}{\leq} \frac{\|\hat{\mathbb{H}}_{\text{od}}(0)\|}{\Delta(0)} + \frac{\|\hat{\mathbb{H}}_{\text{od}}(t)\|}{\Delta(t)} + 2 \frac{\|\dot{\hat{\mathbb{H}}}_{\text{od}}(0)\|}{\Delta^2(0)} + 2 \frac{\|\dot{\hat{\mathbb{H}}}_{\text{od}}(t)\|}{\Delta^2(t)} + \int_0^t \frac{1}{\Delta^2(t)} \left\| \frac{d^2 \hat{\mathbb{H}}_{\text{od}}(t)}{dt^2} \right\| dt \tag{B19}
\end{aligned}$$

where the approximation 1 is obtained by the integration by part, replacing $U_d(\tau, t)$ with $\frac{dU_d(\tau, t)}{d\tau} \hat{\mathbb{H}}_{\text{d}}^{-1}$ and that $\langle m_\alpha | \hat{\mathbb{H}}_{\text{d}}^{-1} | \psi_0 \rangle \sim 1/\Delta_\alpha$; the equality 2 is obtained by two more integration by parts for the last integration from the previous line, and the inequality 3 is given by the triangle inequality. The middle two terms of Eq. (B19) are shown (see SM. B 2) to be at least one magnitude smaller than the left of the terms in either on-resonant or off-resonant regime and can thus be omitted in our final leakage bound:

$$L_{\text{tot}} = \frac{\|\hat{\mathbb{H}}_{\text{od}}(0)\|}{\Delta(0)} + \frac{\|\hat{\mathbb{H}}_{\text{od}}(t)\|}{\Delta(t)} + \int_0^t \frac{1}{\Delta^2(t)} \left\| \frac{d^2 \hat{\mathbb{H}}_{\text{od}}(t)}{dt^2} \right\| dt \tag{B20}$$

We now compare different terms of the leakage bound of Eq. (9) in the main text in both on-resonant and off-resonant frequency regimes separately. First, consider the off-resonant frequency regime such that the Fourier components of the Hamiltonian modulation has a frequency range upper bounded by a value much smaller than Δ such that for any n th order time-derivative we have $\frac{d^n \|\hat{\mathbb{H}}_{\text{od}}\|/dt^n}{\|\hat{\mathbb{H}}_{\text{od}}\|} \sim \epsilon^n \ll \Delta^n$, where the modulation rate of the system Hamiltonian is much smaller than the minimum energy gap separating different energy subspaces. The TSWT assumption in off-resonant regimes implies: $\|\hat{\mathbb{H}}_{\text{d}}\| \sim \epsilon$ and $\|\hat{\mathbb{H}}_{\text{od}}\| \sim \epsilon^3/\Delta^2$. Moreover, in the off-resonant regime, the total run time T obeys $1/T \ll \Delta$ to guarantee the modulation frequency to be smaller than the energy gap. The first two terms in Eq. (B19) $\frac{\|\hat{\mathbb{H}}_{\text{od}}(0)\|}{\Delta(0)} + \frac{\|\hat{\mathbb{H}}_{\text{od}}(t)\|}{\Delta(t)} \sim O(\frac{\epsilon^3}{\Delta^3})$ dominate in this regime since they separated from the left of the terms by a factor of $1/\Delta$ with $\Delta = \min_t \Delta(t)$.

Second, consider the on-resonant frequency regime where the frequency components of the Hamiltonian modulation is of similar magnitudes as the energy gap such that: $\frac{d^n \|\hat{\mathbb{H}}_{\text{od}}\|/dt^n}{\|\hat{\mathbb{H}}_{\text{od}}\|} \sim \Delta^n$, where unwanted couplings between the qubit subspace and a higher energy subspace is of approximately the same frequency as the energy gap. TSWT assumption still holds with the amplitudes of the time-dependent Hamiltonians obeying $\|\hat{H}_1\| \sim \|\hat{H}_2\| \sim \epsilon$. The last term in Eq. (B19) $\int_0^t \frac{1}{\Delta^2(t)} \left\| \frac{d^2 \hat{\mathbb{H}}_{\text{od}}(t)}{dt^2} \right\| dt \sim O(\frac{\epsilon^3}{\Delta^3})$ dominate in this regime since they separated from the left of the terms by a factor of $1/\Delta$.

Non-adiabatic Leakage Bound:

A generalized adiabatic theorem below bounds the leakage amplitude into higher energy subspaces.

Theorem 2. Let $\hat{H}(s)$ be a twice differentiable Hamiltonian parametrized by a unit-free re-scaled time $s \in [0, 1]$ comprising three parts: $\hat{H}(s) = H_0 + \hat{\mathbb{H}}_d(s) + \hat{\mathbb{H}}_{od}(s)$. The time-invariant term $\hat{H}_0 = \sum_{\alpha=0}^{\infty} \sum_{m \in \Omega_\alpha} E_\alpha |m\rangle \langle m|$ ensures large constant energy gap between the lowest energy subspace Ω_0 and other higher energy subspaces. The time-varying term $\hat{\mathbb{H}}_d(s)$ accounts for couplings within each non-degenerate subspace Ω_α and $\hat{\mathbb{H}}_{od}(s)$ accounts for the coupling between different subspaces. There is a separation between the energy gap and inter/intra-subspace coupling: $\Delta = \min_\alpha |E_\alpha - E_0| \gg |\hat{\mathbb{H}}_d(s)| \sim |\hat{\mathbb{H}}_{od}(s)| \sim \delta$. Let $|\phi_0(s)\rangle = \sum_{m \in \Omega_0} a_m(s) |m\rangle$ be an instantaneous eigenstate in the lowest energy subspace Ω_0 at physical time sT . Let $|\psi(s)\rangle$ be the state evolved from the same initial state $|\phi_0(0)\rangle$ at time $s = 0$ under the total Hamiltonian $\hat{H}(s)$ to time s . We have the following inequality that bound the difference between these two states at the final time T by:

$$\begin{aligned} L_{\text{non-adiabatic}} \leq & \frac{1}{T} \left[\frac{1}{\Delta^2(s)} \left(\left\| \frac{d\hat{\mathbb{H}}_{od}(s)}{ds} \right\| + T \left\| [\hat{\mathbb{H}}_d(s), \hat{\mathbb{H}}_{od}(s)] \right\| \right) \Big|_{s=1} + \frac{1}{\Delta^2(s)} \left\| \frac{d\hat{\mathbb{H}}_{od}(s)}{ds} \right\| \right. \\ & + T \left\| [\hat{\mathbb{H}}_d(s), \hat{\mathbb{H}}_{od}(s)] \right\| \Big|_{s=0} \Big] + \int_0^1 \frac{5}{\Delta^3(s)} \left(\left\| \frac{d\hat{\mathbb{H}}_{od}(s)}{ds} \right\| + T \left\| [\hat{\mathbb{H}}_d(s), \hat{\mathbb{H}}_{od}(s)] \right\| \right)^2 ds \\ & + \int_0^1 \frac{1}{\Delta^2(s)} \left(T \left\| [\hat{\mathbb{H}}_d(s), [\hat{\mathbb{H}}_d(s), \hat{\mathbb{H}}_{od}(s)]] \right\| + 2 \left\| [\hat{\mathbb{H}}_d(s), \frac{d\hat{\mathbb{H}}_{od}(s)}{ds}] \right\| + 2 \left\| \left[\frac{d\hat{\mathbb{H}}_d(s)}{ds}, \hat{\mathbb{H}}_{od}(s) \right] \right\| \right. \\ & \left. + \frac{1}{T} \left\| \frac{d^2 \hat{\mathbb{H}}_{od}(s)}{ds^2} \right\| \right) ds, \end{aligned} \quad (\text{B21})$$

where we choose appropriate global phase for the initial state following the convention in [41].

Proof: The proof is a generalization of Goldstone in Ref. [41] to account for inter-subspace dynamics induced by $\hat{\mathbb{H}}_d$ and intra-subspace coupling induced by $\hat{\mathbb{H}}_{od}$. To begin with, we change from Schrödinger picture basis $|\psi(s)\rangle$ to the interaction picture basis $|\tilde{\psi}(s)\rangle$. Let us define the unitary evolution under the time-dependent diagonal Hamiltonian $\hat{\mathbb{H}}_d(s)$ as

$$U_d(s, 0) = \mathbb{T}[e^{-iT \int_0^1 \hat{\mathbb{H}}_d(s) ds}] \quad (\text{B22})$$

which includes quantum dynamics within each subspace Ω_α and satisfies the Schrödinger's equation:

$$\frac{d}{ds} U_d(s, 0) = -iT(\hat{\mathbb{H}}_d(s))U_d(s, 0). \quad (\text{B23})$$

In the rotated basis $|\tilde{\psi}(s)\rangle = U_d(s, 0)|\psi(s)\rangle$, the quantum dynamics induced by $\hat{\mathbb{H}}_d(s)$ within each subspace is absent since:

$$\frac{i}{T} \frac{d}{ds} |\tilde{\psi}(s)\rangle = (\hat{H}_0 + \hat{\mathbb{H}}_d(s) + \hat{\mathbb{H}}_{od}(s))U_d(s, 0)|\tilde{\psi}(s)\rangle, \quad (\text{B24})$$

$$\frac{i}{T} \frac{d}{ds} (U_d(s, 0)|\tilde{\psi}(s)\rangle) + U_d(s, 0) \frac{d}{ds} |\tilde{\psi}(s)\rangle = (\hat{H}_0 + \hat{\mathbb{H}}_d(s) + \hat{\mathbb{H}}_{od}(s))U_d(s, 0)|\tilde{\psi}(s)\rangle, \quad (\text{B25})$$

$$\rightarrow \frac{d}{ds} |\tilde{\psi}(s)\rangle = U_d(0, s)(\hat{H}_0 + \hat{\mathbb{H}}_{od}(s))U_d(s, 0)|\tilde{\psi}(s)\rangle = \hat{\hat{H}}(s)|\tilde{\psi}(s)\rangle, \quad (\text{B26})$$

$$\hat{\hat{H}}(s) = U_d(0, s)(\hat{H}_0 + \hat{\mathbb{H}}_{od}(s))U_d(s, 0) = \hat{H}_0 + U_d(0, s)\hat{\mathbb{H}}_{od}(s)U_d(s, 0) \quad (\text{B27})$$

where we use $\hat{\hat{H}}(s)$ to represent the effective Hamiltonian in the rotated basis. Now we continue to establish the adiabatic theorem in the rotated basis: if the system Hamiltonian changes slow enough, the transition from the ground state living in the lowest energy subspace Ω_0 to an excited state in higher energy subspace is negligible.

Let $|\phi_n(s)\rangle$ be the instantaneous energy eigenstate of the effective Hamiltonian in the interaction picture :

$$\hat{\hat{H}}(s)|\phi_n(s)\rangle = \tilde{E}_n(s)|\phi_n(s)\rangle. \quad (\text{B28})$$

The caveat is here the eigenvalues $\{\tilde{E}_n\}$ are that of the effective Hamiltonian $\hat{H}_0 + U_d(0, s)\hat{\mathbb{H}}_{\text{od}}(s)U_d(s, 0)$, which differs from the original energies $\{E_n\}$ of the static Hamiltonian $\hat{H}_0 = \sum_{n=0}^{\infty} E_n|\phi_n\rangle\langle\phi_n|$ by a factor of $O(\frac{\epsilon^3}{\Delta^3})$ under our assumptions.

By appropriately choosing the global phase $e^{i\int_0^T E_0(t)dt}$ of initial state, we make sure that the lowest energy state in the subspace Ω_0 has an eigenvalue $E_0 = 0$ and will thus remain zero through out the evolution:

$$\hat{H}(s)|\tilde{\phi}_0(s)\rangle = 0. \quad (\text{B29})$$

The deviation from the adiabatic evolution between the actual state and the instantaneous eigenstate is measured by

$$\delta(T) = |\tilde{\psi}(T)\rangle - |\tilde{\phi}_0(T)\rangle = U_T(1, 0)|\tilde{\phi}_0(0)\rangle - |\tilde{\phi}_0(T)\rangle, \quad (\text{B30})$$

where we use $U_T(1, 0)$ as the unitary transformation induced by the effective Hamiltonian in the rotated basis $\hat{H}(s)$ for time T :

$$U_T(1, s) = \mathbb{T}[e^{-iT\int_s^1 \hat{H}(s)ds}], \quad (\text{B31})$$

which also obeys the Schrödinger's equation:

$$\frac{d}{ds}U_T(1, s) = iTU_T(1, s)\hat{H}(s) = iTU_T(1, s)(\hat{H}_0 + U_d(0, s)\hat{\mathbb{H}}_{\text{od}}(s)U_d(s, 0)). \quad (\text{B32})$$

Similar to proof in Goldstone[41], we re-write the adiabatic deviation in Eq. (B30) as

$$\delta(T) = \int_0^1 \frac{d}{ds} [U_T(1, s)|\tilde{\phi}_0(s)\rangle] ds \quad (\text{B33})$$

After differentiating by parts, we have

$$\delta(T) = \int_0^1 ds \frac{d}{ds} [U_T(1, s)] |\tilde{\phi}_0(s)\rangle + \int_0^1 ds U_T(1, s) \frac{d}{ds} |\tilde{\phi}_0(s)\rangle \quad (\text{B34})$$

Inserting Schrödinger Eq. (B32) into Eq. (B34) we have

$$\begin{aligned} \delta(T) &= iT \int_0^1 ds U_T(1, s) \hat{H}(s) |\tilde{\phi}_0(s)\rangle + T \int_0^1 ds U_T(1, s) \frac{d}{ds} |\tilde{\phi}_0(s)\rangle \\ &= T \int_0^1 ds U_T(1, s) \frac{d}{ds} |\tilde{\phi}_0(s)\rangle, \end{aligned} \quad (\text{B35})$$

where we simplify the expression with the fact that $|\tilde{\phi}_0(s)\rangle$ is the zero eigenvalue instantaneous eigenstate of the rotated Hamiltonian. To simplify the second term, we differentiate Eq. (B29) with respect to s on both side to obtain:

$$\frac{d\hat{H}(s)}{ds} |\tilde{\phi}_0(s)\rangle + \hat{H}(s) \frac{d}{ds} |\tilde{\phi}_0(s)\rangle = 0, \quad (\text{B36})$$

$$\rightarrow \hat{H}(s) \frac{d}{ds} |\tilde{\phi}_0(s)\rangle = -\frac{d}{ds} [\hat{H}_0 + U_d(0, s)\hat{\mathbb{H}}_{\text{od}}(s)U_d(s, 0)] |\tilde{\phi}_0(s)\rangle = -\frac{d\hat{H}_{\text{od}}(s)}{ds} |\tilde{\phi}_0(s)\rangle, \quad (\text{B37})$$

$$\rightarrow \frac{d}{ds} |\tilde{\phi}_0(s)\rangle = -\hat{G}' \frac{d\hat{H}_{\text{od}}(s)}{ds} |\tilde{\phi}_0(s)\rangle \quad (\text{B38})$$

where we use the fact that \hat{H}_0 is a constant and the short hand notation $\hat{H}_{\text{od}}(s) = U_d(0, s)\hat{\mathbb{H}}_{\text{od}}(s)U_d(s, 0)$ and the inverse of the effective Hamiltonian $\hat{G}' = \hat{H}^{-1}$ as

$$\hat{G}' = \sum_{n \neq 0} \frac{1}{\hat{E}_n} |\phi_n(s)\rangle \langle \phi_n(s)| \approx \sum_{n \neq 0} \frac{1}{E_n} |\phi_n(s)\rangle \langle \phi_n(s)| + O\left(\frac{\epsilon^4}{\Delta^3}\right) \approx \hat{G}', \quad (\text{B39})$$

where we use the same order of magnitude analysis as Eq. (B28): the rotated basis energy gap between different energy subspaces is the same as the original energy gap up to the order $O(\frac{\epsilon^4}{\Delta^3})$ with $\epsilon \ll \Delta$. Insert Eq. (B32) and Eq. (B38) into Eq. (B35) and apply integration by parts, we obtain:

$$\delta(T) = \int_0^1 \frac{1}{iT} \frac{dU_T(1, s)}{ds} \hat{H}^{-1} \left(-\hat{G}' \frac{d\hat{H}_{\text{od}}(s)}{ds} \right) |\tilde{\phi}_0(s)\rangle, \quad (\text{B40})$$

$$= \frac{i}{T} U_T(1, s) (\hat{G}')^2 \frac{d\hat{H}_{\text{od}}(s)}{ds} \Big|_{s=0}^{s=1} - \frac{i}{T} \int_0^1 ds U_T(1, s) \frac{d}{ds} \left[(\hat{G}')^2 \frac{d\hat{H}_{\text{od}}(s)}{ds} |\tilde{\phi}_0(s)\rangle \right]. \quad (\text{B41})$$

Now using the results in Ref. [41], it is straight forward to give the bound on the magnitude of the adiabatic deviation given in Eq. (B41) as

$$\begin{aligned} \|\delta(T)\| &\leq \frac{1}{T} \left[\left\| (\hat{G}')^2 \frac{d\hat{H}_{\text{od}}(s)}{ds} \right\|_{s=0} + \left\| (\hat{G}')^2 \frac{d\hat{H}_{\text{od}}(s)}{ds} \right\|_{s=1} + \int_0^1 \left\| \frac{d}{ds} (\hat{G}')^2 \frac{d\hat{H}_{\text{od}}(s)}{ds} |\tilde{\phi}_0(s)\rangle \right\| ds \right] \\ &\leq \frac{1}{T} \left[\left\| (\hat{G}')^2 \frac{d\hat{H}_{\text{od}}(s)}{ds} \right\|_{s=0} + \left\| (\hat{G}')^2 \frac{d\hat{H}_{\text{od}}(s)}{ds} \right\|_{s=1} \right] \\ &\quad + \frac{1}{T} \left[\int_0^1 ds \left(5 \left\| (\hat{G}')^3 \right\| \left\| \frac{d\hat{H}_{\text{od}}(s)}{ds} \right\|^2 + \left\| (\hat{G}')^2 \right\| \left\| \frac{d^2 \hat{H}_{\text{od}}(s)}{ds^2} \right\| \right) \right]. \end{aligned} \quad (\text{B42})$$

Expanding the derivative of the off-diagonal Hamiltonian in the rotated basis we have

$$\begin{aligned} \frac{d\hat{H}_{\text{od}}(s)}{ds} &= \frac{d}{ds} \left(U_d(0, s) \hat{\mathbb{H}}_{\text{od}}(s) U_d(s, 0) \right), \quad (\text{B43}) \\ &= iT U_d(0, s) \hat{\mathbb{H}}_d(s) \hat{\mathbb{H}}_{\text{od}}(s) U_d(s, 0) + U_d(0, s) \frac{d\hat{\mathbb{H}}_{\text{od}}(s)}{ds} U_d(s, 0) \\ &\quad - iT U_d(0, s) \hat{\mathbb{H}}_{\text{od}}(s) \hat{\mathbb{H}}_d(s) U_d(s, 0), \\ &= iT U_d(0, s) [\hat{\mathbb{H}}_d(s), \hat{\mathbb{H}}_{\text{od}}(s)] U_d(s, 0) + U_d(0, s) \frac{d\hat{\mathbb{H}}_{\text{od}}(s)}{ds} U_d(s, 0). \end{aligned}$$

This and the triangle inequality gives us an upper bound on the norm of the term:

$$\left\| \frac{d\hat{H}_{\text{od}}(s)}{ds} \right\| \leq \left\| \frac{d\hat{\mathbb{H}}_{\text{od}}(s)}{ds} \right\| + T \left\| [\hat{\mathbb{H}}_d(s), \hat{\mathbb{H}}_{\text{od}}(s)] \right\|. \quad (\text{B44})$$

Differentiate Eq. (B43) with respect to s once more we obtain:

$$\begin{aligned}
\frac{d^2 \hat{H}_{\text{od}}(s)}{ds^2} &= -T^2 U_d(0, s) \hat{\mathbb{H}}_d^2(s) \hat{\mathbb{H}}_{\text{od}}(s) U_d(s, 0) + iTU_d(0, s) \frac{d\hat{\mathbb{H}}_d(s)}{ds} \hat{\mathbb{H}}_{\text{od}}(s) U_d(s, 0) \\
&+ iTU_d(0, s) \hat{\mathbb{H}}_d(s) \frac{d\hat{\mathbb{H}}_{\text{od}}(s)}{ds} U_d(s, 0) + T^2 U_d(0, s) \hat{\mathbb{H}}_d(s) \hat{\mathbb{H}}_{\text{od}}(s) \hat{\mathbb{H}}_d(s) U_d(s, 0) \\
&+ iTU_d(0, s) \hat{\mathbb{H}}_d(s) \frac{d\hat{\mathbb{H}}_{\text{od}}(s)}{ds} U_d(s, 0) + U_d(0, s) \frac{d^2 \hat{\mathbb{H}}_{\text{od}}(s)}{ds^2} U_d(s, 0) - iTU_d(0, s) \frac{d\hat{\mathbb{H}}_{\text{od}}(s)}{ds} \hat{\mathbb{H}}_d(s) U_d(s, 0) \\
&+ T^2 U_d(0, s) \hat{\mathbb{H}}_d(s) \hat{\mathbb{H}}_{\text{od}}(s) \hat{\mathbb{H}}_d(s) U_d(s, 0) - iTU_d(0, s) \frac{d\hat{\mathbb{H}}_{\text{od}}(s)}{ds} \hat{\mathbb{H}}_d(s) U_d(s, 0) \\
&- iTU_d(0, s) \hat{\mathbb{H}}_{\text{od}}(s) \frac{d\hat{\mathbb{H}}_d(s)}{ds} U_d(s, 0) - T^2 U_d(0, s) \hat{\mathbb{H}}_{\text{od}}(s) \hat{H}_d^2(s) U_d(s, 0) \\
&= T^2 U_d(0, s) [\hat{\mathbb{H}}_d(s), [\hat{\mathbb{H}}_d(s), \hat{\mathbb{H}}_{\text{od}}(s)]] U_d(s, 0) + i2TU_d(0, s) [\hat{\mathbb{H}}_d(s), \frac{d\hat{\mathbb{H}}_{\text{od}}(s)}{ds}] U_d(s, 0) \\
&+ U_d(0, s) \frac{d^2 \hat{\mathbb{H}}_{\text{od}}(s)}{ds^2} U_d(s, 0) + i2TU_d(0, s) [\frac{d\hat{\mathbb{H}}_d(s)}{ds}, \hat{\mathbb{H}}_{\text{od}}(s)] U_d(s, 0)
\end{aligned} \tag{B45}$$

This give us the upper bound on the second derivative in the non-adiabatic deviation as:

$$\begin{aligned}
\left\| \frac{d^2 \hat{H}_{\text{od}}(s)}{ds^2} \right\| &\leq T^2 \| [\hat{\mathbb{H}}_d(s), [\hat{\mathbb{H}}_d(s), \hat{\mathbb{H}}_{\text{od}}(s)]] \| + 2T \| [\hat{\mathbb{H}}_d(s), \frac{d\hat{\mathbb{H}}_{\text{od}}(s)}{ds}] \| \\
&+ 2T \| [\frac{d\hat{\mathbb{H}}_d(s)}{ds}, \hat{\mathbb{H}}_{\text{od}}(s)] \| + \left\| \frac{d^2 \hat{\mathbb{H}}_{\text{od}}(s)}{ds^2} \right\|.
\end{aligned} \tag{B46}$$

Inserting Eq. (B44) and Eq. (B46) into Eq. (B42) completes the proof.

We now evaluate the magnitudes of each term of our non-adiabatic leakage bound in off-resonant regime. Under the same assumption as our analysis for coherent leakage errors, we can bound the order of magnitudes of non-adiabatic leakage errors from Eq. (B21) by $\|\hat{\mathbb{H}}_d \hat{\mathbb{H}}_{\text{od}}\|/\Delta^2 \sim O(\epsilon^4/\Delta^4)$. It is one order lower than that from the direct coupling leakage bound in Eq. (3) which is of the order $\|\hat{\mathbb{H}}_{\text{od}}\|/\Delta \sim O(\epsilon^3/\Delta^3)$. As the result, off-resonant leakage errors are dominated by the direct coupling leakage errors.

Appendix C: Control Filter Design

In this section, we describe in greater detail the design of the control filters used to suppress the first term of the leakage error bounded of Eq. (3) in the main text. Each time-dependent control trajectory is discretized into N steps in piece-wise constant representation, with neighboring steps separated by a small time duration Δt . The modulation rate of the control signal is determined by this smallest time step according to $F_{\text{sample}} = 1/\Delta t$. We treat $\hbar = 1$ throughout our discussion. Since the first term of leakage bound from Eq. (3)

$$\int_0^1 \frac{1}{\Delta^2(s)} \frac{1}{T} \left\| \frac{d^2 \hat{\mathbb{H}}_{\text{od}}(s)}{ds^2} \right\| ds \tag{C1}$$

is proportional to the second time-derivative of the block-off-diagonal Hamiltonian after TSWT, to suppress it to a small value, we need to ensure that the frequency component of any control action proposed by RL agent proposed is sufficiently small compared to the energy gap Δ .

Without affecting the Markovianity of the control problem while limiting the frequency components of the control, we choose to apply a two pole normalized double exponential smoothing filter [42] to the proposed control

action. At each time step $1 \leq n \leq N$, the new control depends not only on the proposed control action \vec{c}_n^{RL} by the RL agent, but also on the control taken in the last step \vec{c}_{n-1} and the last last step \vec{c}_{n-2} according to:

$$\vec{c}_n = a_1 \vec{c}_n^{RL} - b_1 \vec{c}_{n-1} - b_2 \vec{c}_{n-2}, \quad (\text{C2})$$

where the filter coefficient is chosen according to the frequency bandwidth B_w of the actuated control and the modulation rate of the control signals as [42]:

$$\alpha = \exp\left[-\frac{\pi B_w}{F_{\text{sample}}}\right], \quad (\text{C3})$$

$$a_1 = (1 - \alpha)^2, \quad b_1 = -2\alpha, \quad b_2 = \alpha^2. \quad (\text{C4})$$

Appendix D: Evaluation of the Average Fidelity

In this section, we present our method of evaluating average fidelity based on previous results of Nielsen [33]. The average fidelity,

$$\bar{F}(\mathcal{E}, U) = \int d\psi \langle \psi | U^\dagger \mathcal{E}(|\psi\rangle\langle\psi|) U | \psi \rangle, \quad (\text{D1})$$

measures the average performance of a quantum gate over a uniform distribution of the input quantum state under the noisy quantum channel \mathcal{E} that describes the actual control realizations. It can be measured in experiment through randomized benchmarking process. Theoretically we evaluate the average fidelity by summing over all possible overlap with Pauli operators as

$$\bar{F}(\mathcal{E}, U) = \frac{\sum_j \text{Tr}[U_{\text{target}} U_j^\dagger U_{\text{target}}^\dagger \mathcal{E}(U_j)] + d^2}{d^2(d+1)}, \quad (\text{D2})$$

where the two-qubit Pauli operator $U_j = (\sigma_1^x)^{h_1} (\sigma_1^z)^{q_1} (\sigma_2^x)^{h_2} (\sigma_2^z)^{q_2}$ with $h_j, q_j \in \{0, 1\}$ satisfies $\text{Tr}[U_j U_k^\dagger] = \delta_{j,k} d$; $d = 4$ is the dimension of the two-qubit subspace dimension; \mathcal{E} is the trace-preserving quantum operation that represents noisy realization of an ideal quantum gate control; U_{target} represents the target quantum gate. It is not hard to see that the sufficient and necessary condition for average fidelity to be one is to have: $\mathcal{E}(\rho) = U_{\text{target}} \rho U_{\text{target}}^\dagger$. We evaluate $\mathcal{E}(\rho)$ of a given control noise model $N(0, \sigma_{\text{noise}})$, a Gaussian random fluctuation in control amplitudes with zero mean and a fixed variance σ_{noise} , by sampling the full control trajectory $\vec{c} + \delta\vec{c}$ under this noise channel and average the evolved quantum state over different instances:

$$\mathcal{E}(\rho) = \mathbb{E}_{\delta\vec{c} \sim N(0, \sigma_{\text{noise}})} U(\vec{c} + \delta\vec{c}) \rho U^\dagger(\vec{c} + \delta\vec{c}). \quad (\text{D3})$$

Such averaging can change a pure state into a mixed state and thus accounts for the magnitude of decoherence induced by stochastic control errors. Fig. 4 of the main text is evaluated under 60 samples per noise model parameter.

-
- [1] R. Barends, *et al.*, *Nature* **508**, 500 (2014).
 - [2] S. Boixo, *et al.*, *arXiv:1608.00263* (2016).
 - [3] C. Neill, *et al.*, *Science* **360**, 195 (2018).
 - [4] R. P. Feynman, *International journal of theoretical physics* **21**, 467 (1982).
 - [5] L. K. Grover, *Proceedings of the twenty-eighth annual ACM symposium on Theory of computing* (ACM, 1996), pp. 212–219.
 - [6] D. Dong, I. R. Petersen, *IET Control Theory & Applications* **4**, 2651 (2010).

- [7] A. Ruschhaupt, X. Chen, D. Alonso, J. Muga, *New Journal of Physics* **14**, 093040 (2012).
- [8] C. Chen, L.-C. Wang, Y. Wang, *The scientific world journal* **2013** (2013).
- [9] F. L. Lewis, D. Liu, *Reinforcement learning and approximate dynamic programming for feedback control*, vol. 17 (John Wiley & Sons, 2013).
- [10] P. Palittapongarnpim, P. Wittek, E. Zahedinejad, S. Vedaie, B. C. Sanders, *Neurocomputing* **268**, 116 (2017).
- [11] Z. K. Nagy, R. D. Braatz, *Journal of process control* **14**, 411 (2004).
- [12] D. Hocker, *et al.*, *Phys. Rev. A* **90**, 062309 (2014).
- [13] S. Machnes, D. J. Tannor, F. K. Wilhelm, E. Assémat, *arXiv preprint arXiv:1507.04261* (2015).
- [14] J. Schulman, P. Moritz, S. Levine, M. Jordan, P. Abbeel, *arXiv:1506.02438* (2015).
- [15] V. Mnih, *et al.*, *International Conference on Machine Learning* (2016), pp. 1928–1937.
- [16] D. Silver, *et al.*, *Nature* **529**, 484 (2016).
- [17] C. Chen, D. Dong, H.-X. Li, J. Chu, T.-J. Tarn, *IEEE transactions on neural networks and learning systems* **25**, 920 (2014).
- [18] M. Bukov, *et al.*, *arXiv:1705.00565* (2017).
- [19] N. Khaneja, T. Reiss, C. Kehlet, T. Schulte-Herbrüggen, S. J. Glaser, *Journal of magnetic resonance* **172**, 296 (2005).
- [20] A. Spörl, *et al.*, *Physical Review A* **75**, 012302 (2007).
- [21] R. Chakrabarti, H. Rabitz, *International Reviews in Physical Chemistry* **26**, 671 (2007).
- [22] K. Moore, M. Hsieh, H. Rabitz, *The Journal of chemical physics* **128**, 154117 (2008).
- [23] J. M. Gambetta, F. Motzoi, S. T. Merkel, F. K. Wilhelm, *Physical Review A* **83**, 012308 (2011).
- [24] J. M. Martinis, M. R. Geller, *Physical Review A* **90**, 022307 (2014).
- [25] E. Zahedinejad, J. Ghosh, B. C. Sanders, *Physical review letters* **114**, 200502 (2015).
- [26] C. J. Wood, J. M. Gambetta, *arXiv preprint arXiv:1704.03081* (2017).
- [27] Y. Goldin, Y. Avishai, *Phys. Rev. B* **61**, 16750 (2000).
- [28] F. Motzoi, J. M. Gambetta, P. Rebentrost, F. K. Wilhelm, *Phys. Rev. Lett.* **103**, 110501 (2009).
- [29] Y. N. Dauphin, *et al.*, *Advances in neural information processing systems* (2014), pp. 2933–2941.
- [30] J. Schulman, S. Levine, P. Abbeel, M. Jordan, P. Moritz, *Proceedings of the 32nd International Conference on Machine Learning (ICML-15)* (2015), pp. 1889–1897.
- [31] Y. Chen, *et al.*, *Phys. Rev. Lett.* **113**, 220502 (2014).
- [32] Y. R. Sanders, J. J. Wallman, B. C. Sanders, *New Journal of Physics* **18**, 012002 (2015).
- [33] M. A. Nielsen, *Physics Letters A* **303**, 249 (2002).
- [34] G. Brockman, *et al.*, *arXiv:1606.01540* (2016).
- [35] J. Ghosh, A. G. Fowler, *Phys. Rev. A* **91**, 020302 (2015).
- [36] F. Vatan, C. Williams, *Phys. Rev. A* **69**, 032315 (2004).
- [37] D. Wecker, M. B. Hastings, M. Troyer, *Phys. Rev. A* **92**, 042303 (2015).
- [38] I. D. Kivlichan, *et al.*, *Phys. Rev. Lett.* **120**, 110501 (2018).
- [39] Z. Jiang, K. J. Sung, K. Kechedzhi, V. N. Smelyanskiy, S. Boixo, *arXiv:1711.05395* (2017).
- [40] D. P. Kingma, J. Ba, *arXiv preprint arXiv:1412.6980* (2014).
- [41] S. P. Jordan, *arXiv:0809.2307* (2008).
- [42] J. O. Smith, *Introduction to digital filters: with audio applications*, vol. 2 (Julius Smith, 2007).